scientific reports

Check for updates

OPEN

INHBA: a mitochondrial-related pan-cell death gene associated with the prognosis and immunity of OSCC

Xiaoting Zhang[1,3], Mouyuan Sun[3]✉, Tao Qiu[3], Di He[4], Tian Zhang[3,4] & Jin Li[2]✉

Oral squamous cell carcinoma (OSCC) is a malignant tumor characterized by both clinical and molecular heterogeneity. Its rising global incidence and mortality rates pose considerable clinical challenges. Accumulating evidence suggests that dysregulation of mitochondria-associated pan-cell death, a process integrating multiple mitochondrial-related cell death modalities, is closely linked to tumor initiation and progression. Nevertheless, the identification of key therapeutic targets among mitochondria-associated pan-cell death-related genes (MAPGs) in OSCC remains an unresolved issue, underscoring the need for further investigation. We systematically investigated the expression patterns, prognostic relevance, and immune microenvironmental features of mitochondria-associated pan-cell death-related genes (MAPGs) in OSCC by integrating data from The Cancer Genome Atlas (TCGA), Gene Expression Omnibus (GEO) datasets (GSE42743, GSE41613, GSE75538, GSE164241, GSE172577, and GSM6339633), and the MitoCarta3.0 database. Using nine machine learning algorithms, we compared the importance and prognostic value of MAPGs and identified INHBA as the most pivotal MAPG. Its predictive power and functional relevance were further explored through enrichment analysis. We validated INHBA mRNA expression levels in clinical OSCC samples using quantitative real-time PCR (qRT-PCR). Pan-cancer analysis was performed to assess the potential of INHBA as a therapeutic target across multiple cancer types. Single-cell RNA sequencing, spatial transcriptomics, and cell-cell communication analyses were integrated to elucidate the spatial distribution of INHBA in OSCC and its crosstalk with the immune microenvironment. Finally, drug sensitivity profiling was conducted using the GDSC and PRISM databases. A total of 19 MAPGs with the greatest prognostic value were screened out. Among them, INHBA emerged as the most critical MAPG, which was overexpressed in HNSCC and strongly correlated with poor prognosis in OSCC patients ($p < 0.05$). Meanwhile, INHBA expression was elevated in cancer-associated fibroblasts (CAFs). Spatial transcriptomic analysis further revealed strong spatial colocalization between INHBA and CAF-localized regions. These results indicated that INHBA primarily functioned within CAFs, especially myCAFs, and may promote OSCC progression through modulation of the immune microenvironment. Elevated INHBA expression served as a prognostic indicator in OSCC, a finding consistent with its prognostic relevance in broader HNSCC analyses. Selumetinib and naltrexone showed high sensitivity in INHBA-high contexts. INHBA is a crucial MAPG that is upregulated in OSCC and mainly functions in CAFs. It likely affects the poor prognosis of OSCC by regulating the immune microenvironment. Selumetinib and naltrexone hold promise as innovative therapeutic agents, potentially opening up new treatment avenues for OSCC patients.

Head and neck squamous cell carcinoma (HNSCC), which arises from the mucosal epithelium of the oral cavity, pharynx, and larynx, represents the sixth most common malignancy worldwide[1]. Over 90% of head and neck cancers are classified as oral squamous cell carcinoma (OSCC), which develops specifically from the oral

[1]Department of Stomatology, Wuhan No.1 Hospital, Wuhan, China. [2]Affiliated Hangzhou First People's Hospital, School of Medicine, Westlake University, Hangzhou, China. [3]Stomatology Hospital, School of Stomatology, Zhejiang University School of Medicine, Zhejiang Provincial Clinical Research Center for Oral Diseases, Zhejiang Key Laboratory of Oral Biomedical, Hangzhou, China. [4]Department of Oral and Maxillofacial Surgery, Second Affiliated Hospital, Zhejiang University School of Medicine, Hangzhou, Zhejiang Province, China. ✉email: sunmouyuan777@zju.edu.cn; lijin_6666@163.com

mucosal epithelium and constitutes approximately 90% of all oral malignancies[2,3]. OSCC significantly impairs vital functions including facial appearance, speech, swallowing, and taste[4]. According to projections from the Global Cancer Observatory (GCO), the incidence of OSCC is expected to rise by about 40% by 2040, with a corresponding increase in mortality[5]. The standard therapeutic approach for OSCC involves surgical resection combined with radiotherapy and chemotherapy. Nevertheless, due to frequent tumor recurrence, metastasis, and treatment resistance, the five-year survival rate for patients with advanced OSCC remains unsatisfactory[6,7]. In recent years, immunotherapy has emerged as a promising strategy that activates, restores, or redirects the host anti-tumor immune response to eliminate tumors, leading to a transformative shift in cancer treatment[8,9]. However, limitations such as side effects, narrow clinical applicability, and low response rates have considerably restricted its widespread use in OSCC[10,11]. Therefore, elucidating the molecular mechanisms underlying OSCC and discovering potential novel therapeutic targets are crucial for improving treatment strategies.

Accumulating evidence indicates that dysregulation of cell death is closely associated with the development and progression of oral squamous cell carcinoma (OSCC)[12,13]. Among the various forms of cell death, apoptosis, autophagy, pyroptosis, ferroptosis, and cuproptosis have been the most extensively investigated in the context of OSCC. Cell death plays a dual, context-dependent role in tumorigenesis, capable of either suppressing or promoting tumor progression depending on the surrounding microenvironment[14]. For example, Zhuang et al. reported that benzoin upregulated NIBAN1 expression in OSCC, promoted autophagy and apoptotic cell death, and thereby suppressed OSCC cell growth, demonstrating potent anti-tumor activity[15]. Similarly, Xia et al. found that REEP6 overexpression promoted OSCC progression through endoplasmic reticulum stress-mediated ferroptosis[16]. However, to date, most studies have focused on genes associated with individual cell death modalities, while the collective role of pan-cell death (PCD)-related genes, encompassing multiple forms of cell death, in OSCC prognosis and immunotherapy remains largely unexplored. Mitochondria serve as crucial organelles that maintain the balance between oxidative stress and cell death during OSCC proliferation[17]. Silvia et al. reported that mitochondrial content regulates the levels of apoptotic proteins in tumor cells, with higher mitochondrial content correlating with increased susceptibility to cell death[18]. In addition, Marte et al. found that circulating mitochondrial DNA (mtDNA) activates TLR9-dependent NF-κB signaling in vivo and promotes cardiomyocyte death[19]. Although the link between mitochondrial genes and cell death has been extensively studied, the precise roles of key mitochondrial-associated pan-cell death genes (MAPGs), defined as the intersection of mitochondrial-related and PCD-related genes, in OSCC pathogenesis, as well as the specific cell subpopulations they target, remain to be elucidated. Therefore, elucidating the potential mechanisms of MAPGs in OSCC may offer valuable insights for immunotherapy, targeted intervention, and prognostic assessment of this malignancy.

Comprehensive multi-omics analyses have substantially advanced our understanding of OSCC heterogeneity, facilitating patient stratification and the development of molecularly targeted therapies, thereby improving treatment outcomes through the identification of key molecular drivers and predictive biomarkers for targeted agents[20–23]. By integrating single-cell RNA sequencing (scRNA-seq) with spatial transcriptomics, we can further pinpoint the specific cell types targeted by MAPGs[24–27]. Concurrently, machine learning approaches, such as least absolute shrinkage and selection operator (LASSO), support vector machines (SVM), and random forests (RF), provide powerful tools for identifying the most prognostically relevant MAPGs[28–32]. The integration of multi-omics profiling with computational approaches provides a powerful strategy to resolve cell type-specific expression patterns in OSCC, enabling the systematic identification of key MAPGs and their associated cellular targets during pathogenesis[33]. This framework establishes a foundation for precision medicine in OSCC treatment.

This study established the clinical relevance of mitochondria-associated pan-cell death genes (MAPGs) in HNSCC, identifying 19 prognostic-related MAPGs. Based on these genes, molecular subtypes of OSCC were constructed to systematically assess their associations with biological functions, immune microenvironment features, and patient survival. By integrating multiple machine learning algorithms, we identified INHBA as a central MAPG, a finding further validated in tumor tissues using quantitative real-time PCR. Single-cell and spatial transcriptomic (ST) analyses revealed that INHBA was predominantly enriched within cancer-associated fibroblasts (CAFs). CellChat analysis indicated that INHBA may promote OSCC progression by modulating CAF-immune cell communication networks. We further examined the relationship between INHBA expression and immune checkpoint markers, immunophenotypic scores, and response to immunotherapy, and performed drug sensitivity screening to identify potential targeted agents. Collectively, these results deepen the understanding of the functional landscape of MAPGs in OSCC and propose new directions for therapeutic development in OSCC patients (Fig. 1).

Materials and methods

Data acquisition

The clinical information and expression data of 502 HNSCC tissues, 44 adjacent normal tissues and corresponding clinical data were downloaded from the Cancer Genome Atlas (TCGA) (http://cancergenome.nih.gov/) database. GEO datasets (GSE42743, GSE41613 and GSE 75538) were downloaded from the GEO (https://www.ncbi.nlm.nih.gov/) database. Single-cell RNA sequencing data were obtained from GEO databases (GSE164241 and GSE172577) and included 8 normal buccal mucosa samples and 6 oral squamous cell carcinoma samples. Spatial transcriptome data were obtained from geo database (GSM6339633). To assess INHBA expression patterns across various cancer types, we searched RNA-Seq data from the TCGA database.

Screening and identification of mitochondria-associated PCD genes

Firstly, mitochondrial associated genes (MIGs) were obtained from the MitoCarta3.0 database[34], and pan-cell death associated genes (PCDGs) were obtained from the literature[35]. Differential expression analysis of

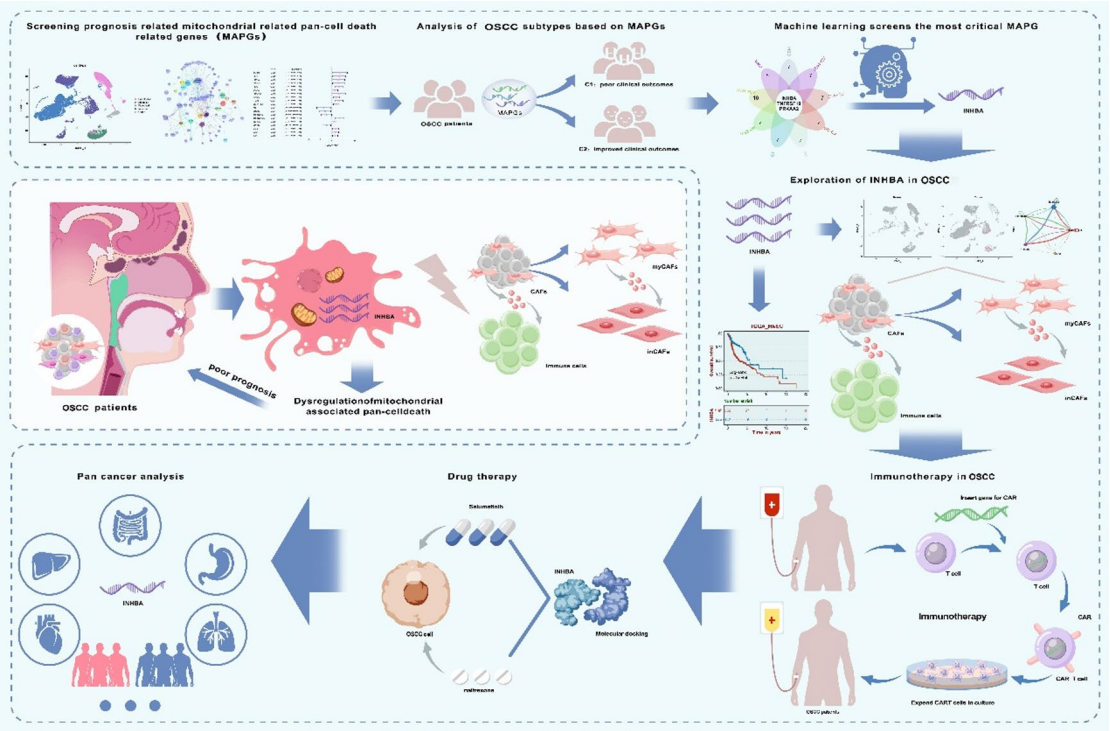

Fig. 1. Mitochondrial associated pan-cell death genes (MAPGs) may be involved in the pathogenesis of OSCC, with unique prognosis and management strategies. Based on 19 key MAPGs, we constructed relevant prognostic features to evaluate their prognostic value for OSCC patients. Among these, INHBA, identified as the most critical MAPG, was selected through nine machine learning algorithms and validated clinically. Notably, OSCC patients with high INHBA expression exhibited poor prognosis. Single-cell and spatial transcriptome analyses revealed that INHBA was predominantly distributed in fibroblasts and may promote the progression of OSCC and influence prognosis by regulating the tumor microenvironment. CAR-T immunotherapy may improve a new therapeutic strategy for OSCC patients with high INHBA expression. Drug sensitivity analyses and molecular docking further demonstrated that selumetinib and naltrexone, by targeting INHBA, could potentially improve OSCC prognosis. Pan-cancer analysis underscored the universal therapeutic significance of targeting INHBA across multiple malignancies.

R-package "limma" (|log FC | ≥1 and FDR < 0.05) was performed to screen MIGs associated with HNSCC disease characteristics. In the same manner, PCDGs associated with HNSCC disease characteristics were screened. Pearson correlation analysis was conducted between differentially expressed MIGs and PCDGs, and mitochondrial-associated pan-cell death genes (MAPGs) were identified using thresholds of correlation coefficient ≥ 0.4 and FDR < 0.001.

Unsupervised cluster analysis based on MAPGs to identify OSCC subtypes

The unsupervised cluster analysis was utilized to classify the 500 OSCC cases based on the 19 MAPGs using the "ConsensusClusterPlus" package. The number of HNSCC subtypes and stability were determined by the Gap statistic and Elbow method. Kaplan–Meier (K-M) Survival curve was used to compare the OS to evaluate the relationship between prognosis and each subtype. Moreover, the immune features and tumor microenvironment (TME) characteristics among the distant MAPGs-based subtypes were compared using the Wilcoxon signed-rank test, which covered the aspects of enrichment levels of immune infiltration cells and tumor microenvironment-related pathways in the tumor samples.

Analysis of functional enrichment

To uncover the underlying biological functions and signaling pathways involved, the Gene Ontology (GO) classification and Kyoto Encyclopedia of Genes and Genomes (KEGG) enrichment analysis were performed using the "clusterProfiler" tool. GSEA using KEGG and Hallmark genes was used to detect signaling pathways in various clusters[36]. FDR < 0.05 was considered statistically significant.

Machine learning filters the most critical MAPGs

We employed nine machine learning algorithms, namely Gradient Boosting (GB), Gradient Boosting with Cross-Validation (GB-CV), Gradient Boosting Machines (GBM), Linear Discriminant Analysis (LDA), Linear Discriminant Analysis with Cross-Validation (LDA-CV), Random Forest (RF), Support Vector Machine (SVM), Support Vector Machine with Cross-Validation (SVM-CV) and LASSO regression to further screen key MAPGs.

LASSO regression was carried out using the glmnet package, generating candidate diagnostic genes via 10-fold cross-validation. The RF model was constructed using the randomForest package. GBM calculation was conducted using the gbm method from the caret R package. The XGBoost calculation was conducted using the xgbTree method from the caret R package. The DT calculation was performed using the rpart R package. GB used the sklearn GradientBoostingClassifier ensemble module for training. KNN used the KNeighborsClassifier from sklearn.neighbors. SVM utilized the Support Vector Classifier (SVC) class of sklearn. svm module with a linear kernel. These three algorithms were implemented through Python (Python version 3.9.7; key libraries: scikit-learn, pandas, numpy, matplotlib, seaborn). To guarantee the strength and dependability of the outcomes, every machine learning model underwent training and validation through a 5-fold cross-validation process. The importance of each feature was determined using permutation importance, and the top 10 features were visualized and saved as PDF files for further analysis.

Differential expression and survival analysis of MAPGs

Wilcoxon symbolic rank test was employed to assess the expression levels of key MAPGs in multiple HNSCC datasets (|log2 (FC) | > 0.5, FDR < 0.05). To objectively classify patients based on INHBA expression, we determined the optimal cutoff value using receiver operating characteristic (ROC) curve analysis. Based on the optimal cut-off values of key MAPGs, all patients were stratified into low- and high-expression groups. Subsequently, survival curves were plotted to compare the survival disparities between these two groups.

Immunological correlation evaluation

The infiltrating immune cell score and immune-related functional activity were calculated by single sample gene set enrichment analysis (ssGSEA). The deconvolution algorithm CIBERSORT was used to estimate the proportion of 22 tumor-infiltrating immune cells in tumor tissue of mixed cell types. ESTIMATE was used to estimate stromal and immune cells in malignant tumors, as well as calculate tumor purity, stromal score, immune score, and ESTIMATE score.

Clustering and annotation of single-cell RNA sequencing data

In single-cell analyses based on RNA sequencing (scRNA-seq) data, principal component analysis (PCA) was applied for reduction and clustering. Cells with < 500 genes, > 4,000 genes, > 15% mitochondrial genes, or > 3% hemoglobin content were excluded. The UMAP diagram visualizes the generated unsupervised cell clusters. To label the cell types within each cluster, we relied on marker genes obtained from previous studies[37,38]. Moreover, heat maps were employed to display and label the differentially expressed genes specific to each cell cluster, thereby highlighting the characteristic genes.

Analysis of intercellular communication

We employed the CellChat R package to investigate intercellular communication patterns. Following the established protocol, we constructed a CellChat object using the normalized count matrix. Permutation tests were performed to assess statistical significance, with default parameters applied across all methodological steps[39]. The CellChatDB human was used for analysis.

Drug sensitivity analysis

The chemotherapeutic response of HNSCC patients was evaluated using the Genomics of Drug Sensitivity in Cancer (GDSC) database (https://www.cancerrxgene.org) and the Profiling of Relative Inhibition Simultaneously in Mixtures (PRISM). The results were visualized as heat maps using the ggplot2 R software package. Molecular docking predictions were carried out using https://www.dockeasy.cn/DockCompound. Visualize the molecular docking results using Discovery Studio version 4.5. The molecular docking results were visualized with Discovery Studio version 4.5. The chemical compositions of drugs were obtained from https://pubchem.ncbi.nlm.nih.gov/#query. The protein structure was retrieved from the RCSB Protein Data Bank (https://www.rcsb.org/) under PDB ID 6Y60. For molecular docking, all protein and ligand files (in XML format) were preprocessed by conversion to PDBQT format. Additionally, all water molecules were removed and polar hydrogen atoms were added to prepare the structures for docking simulations. Affinity values, expressed in kilocalories per mole, indicated the binding degree of two substances. Lower affinity (kcal/mol) values corresponded to higher stability of ligand - receptor binding.

Patients and tissue specimens

HNSCC and normal tissue samples were collected from patients with HNSCC who underwent extensive surgery at the Second Affiliated Hospital of Zhejiang University School of Medicine. The study complied with all applicable local, national and global guidelines. Obtain informed written consent from all individuals providing human patient samples prior to donation. This study was approved by the Human Research Ethics Committee of the Second Affiliated Hospital of Zhejiang University School of Medicine (Ethics No. 20250631).

The inclusion and exclusion criteria for clinical samples used in this study are outlined below:

Inclusion Criteria: ① Pathologically confirmed diagnosis of HNSCC, with no prior treatment (treatment-naïve); ② No surgical history within the two years preceding study enrollment;③ Normal function of major organs (e.g., heart, kidneys, liver); ④ Absence of significant gastrointestinal or metabolic disorders; ⑤ No history of chemotherapy within the two years prior to inclusion; ⑥ Provision of informed consent by the patient and their family; ⑦ Availability of complete clinical and follow-up data.

Exclusion Criteria:①Patients with secondary primary cancers at other sites;②Severe cardiovascular or cerebrovascular diseases;③Active or uncontrolled severe infectious diseases;④Presence of obstructive

gastrointestinal or respiratory tract conditions;⑤Voluntary withdrawal or loss to follow-up during the study period.

Real-time polymerase chain reaction (RT-qPCR) analysis

Total RNA was extracted from tumor tissues and normal control tissues using TRIzol reagent (Invitrogen, USA), and cDNA samples were synthesized using superscript II first-strand cDNA synthesis kit (TaKaRa, Japan)[40]. The expression level of INHBA was determined by real-time fluorescence quantification, with GAPDH serving as the internal control. The relative mRNA expression was determined using the comparative Ct (ΔΔCt) method. The primers used for RT-qPCR analysis are shown in Table S1.

Statistics analysis

All statistical analyses were conducted using R software (version 4.2.1), Python version 3.9.7, GraphPad Prism 8 (GraphPad Software, United States), and PASS 27.0 software. The specific R studio software packages used in each chapter are described. A p - value < 0.05 was considered statistically significant. To control for potential false positives, we applied multiple test correction using the Benjamini-Hochberg false discovery rate (FDR) procedure to relevant statistical analyses in this study. These included differential expression analysis performed with the "limma" R package, functional enrichment analysis, and evaluation of key MAPG expression levels across multiple HNSCC datasets using the Wilcoxon signed-rank test. An adjusted p-value (FDR) of < 0.05 was considered statistically significant in all these analyses.

Results

Screening of mitochondria-associated pan-cell death genes (MAPGs) in OSCC

To investigate the cell type-specific expression patterns of mitochondria-associated pan-cell death-related genes (MAPGs) in OSCC, we analyzed single-cell RNA sequencing (scRNA-seq) data (Fig. 2A, S1). Using the UMAP algorithm, we classified the major cell populations into four principal compartments: epithelial cells, endothelial cells, fibroblasts, and immune cells (Fig. 2A,B). Comparative analysis revealed an expansion of immune and epithelial cell compartments in OSCC tissues compared to paracancerous tissues, whereas fibroblast and endothelial cell compartments were reduced (Fig. 2C,D). AUCell scoring demonstrated active expression of both mitochondrial-related genes (MIGs) and pan-cell death-related genes (PCDGs) particularly in epithelial cells and fibroblasts of OSCC (Fig. 2E). Differential expression analysis of MIGs and PCDGs was visualized using volcano plots (Fig. 2F,G). By integrating correlation analysis, LASSO regression, and multivariate Cox regression, we identified 19 mitochondria-associated pan-cell death genes (MAPGs) with significant prognostic

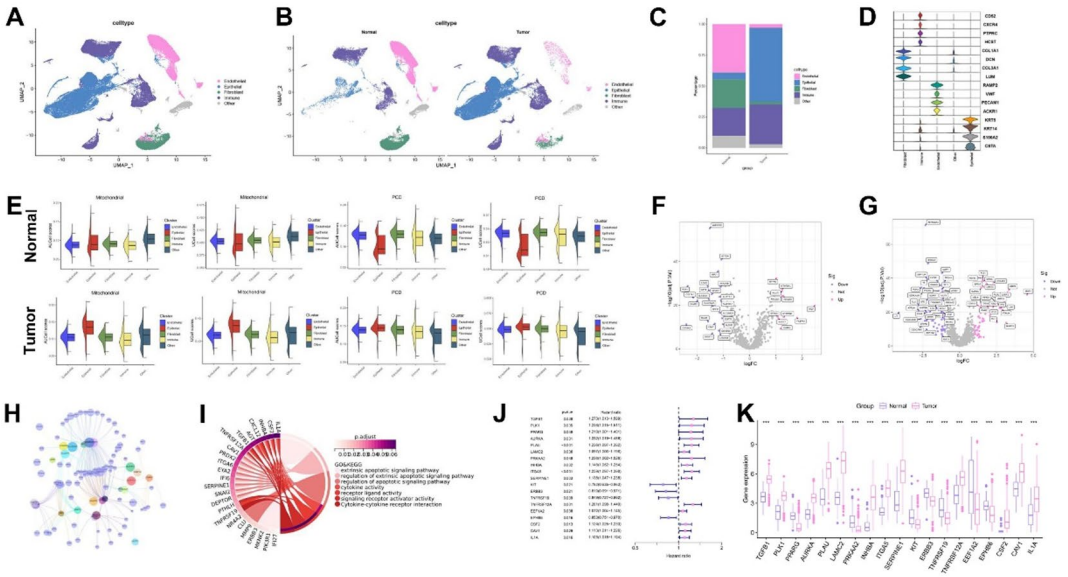

Fig. 2. Screening of major cell types and mitochondria-associated pan-cell death genes (MAPGs) in OSCC. (**A**) UMAP visualization of major cell types. (**B**) UMAP plots contrasting normal and malignant cells in OSCC. (**C**) Bar graph depicting the relative proportions of cell types. (**D**) Marker genes expressed within the four major cell compartments. (**E**) Scores of OSCC related to mitochondrial and cell death processes in normal and malignant cells. (**F**) Volcano plot illustrating differentially expressed mitochondria-related genes (MIGs) in OSCC. (**G**) Volcano plot showing differentially expressed pan-cell death-related genes (PCDGs) in OSCC. (**H**) Correlation analysis between MIGs and PCDGs. (**I**) The gene functional enrichment analysis (GO and KEGG analysis). (**J**) Univariate Cox regression analysis identifying 19 MAPGs significantly associated with prognosis. (**K**) Expression levels of MAPGs in normal group and HNSCC group. GO, Gene Ontology; KEGG, Kyoto Encyclopedia of Genes and Genomes. *$p < 0.05$, **$p < 0.01$, ***$p < 0.001$, ****$p < 0.0001$.

value for OSCC patients (Fig. 2H–K). However, the correlation between MAPGs expression and clinical features in OSCC still needed further analysis.

OSCC subtype analysis based on MAPGs

To explore the prognostic relevance of MAPGs, we performed unsupervised consensus clustering and categorized all OSCC samples into two distinct subtypes (C1 and C2) (FigS2.A-I; Fig. 3A). Principal component analysis (PCA) confirmed clear separation between the two subtypes (Fig. 3B). Kaplan-Meier survival analysis revealed that patients in the C2 subtype had significantly better survival outcomes than those in C1 (Fig. 3C).

We further characterized the tumor microenvironment (TME) differences between MAPGs-based subtypes. Subtype C1 was enriched with T cells CD4 memory resting, NK cells resting, macrophages, dendritic cells activated, mast cells activated and neutrophils. C2 group enriched B cells naive, plasma cells, T cells CD8, T cells CD4 memory activated, T cells regulatory and mast cells resting (Fig. 3E,F). Single-sample gene set enrichment analysis (ssGSEA) revealed that apoptosis, glycolysis, IL6-JAK-STAT3 signaling, Notch signaling, PI3K-AKT-mTOR signaling, TGF-β signaling, and TNFα signaling via NF-κB were significantly enriched in C1 (Fig. 3G). Compared with C2, C1 showed higher expression of chemokine-related genes (CCL3, CCL7, CCL8, CCL11, CCL13, CCL21, CCL24, CCL26, CXCL1, CXCL2, CXCL3, CXCL5, CXCL6, CXCL10, CXCL11, CXCL14) and increased CTLA4 expression (Fig. 3H,I). Combined with the immune score results, we found that the immune score was higher in C1 (Fig. 3D,K–M), suggesting the presence of an immunosuppressive TME, which may contribute to its poorer prognosis, while C1 might be more sensitive to immunotherapy. The results of GO enrichment analysis and KEGG pathway analysis showed that molecular metabolism, protein binding and PI3K-AKT signaling pathways were more prominent in C1 group (Fig. 3O,P). Collectively, these results suggested that key MAPGs might promote the progression of OSCC by regulating the tumor immune microenvironment, although the specific mechanism requires further exploration.

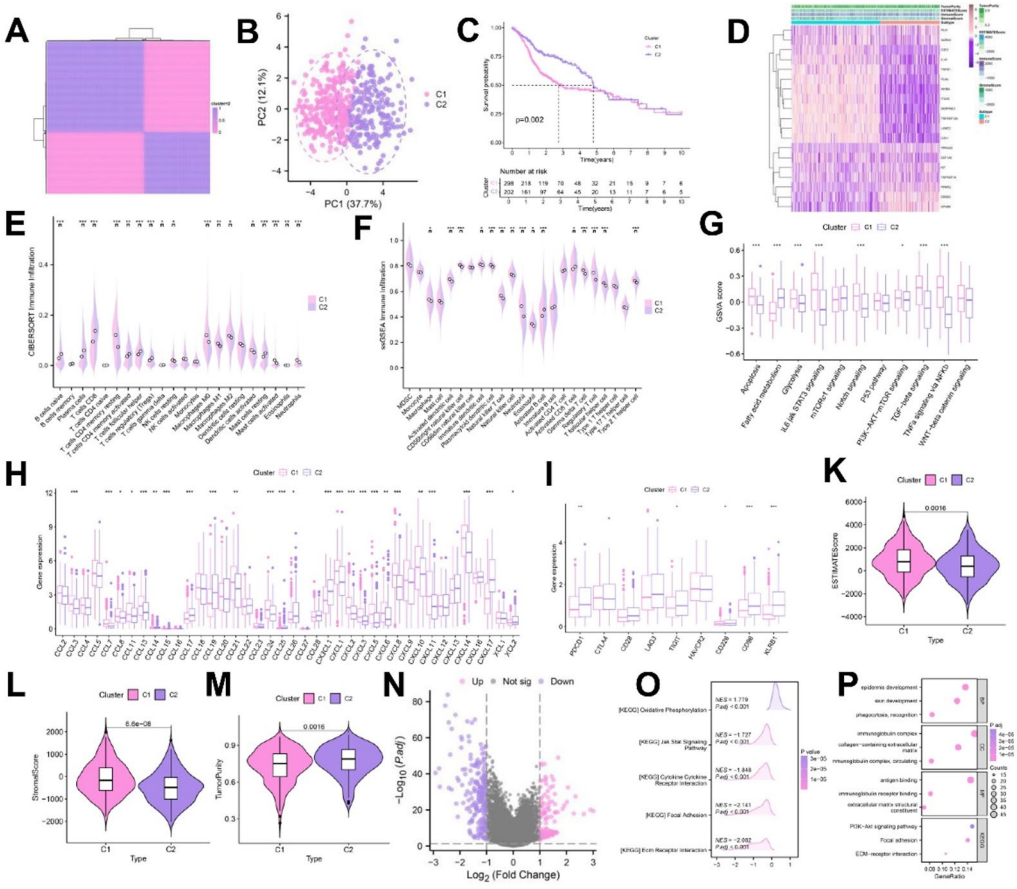

Fig. 3. Analysis of OSCC subtypes based on MAPGs. (**A**) Two MAPGs-related molecular clusters were identified by NMF cluster analysis. (**B**) PCA analysis of distinct MAPGs-related molecular clusters. (**C**) Kaplan-Meier curve of differential survival between C1 and C2 groups. (**D**) Heatmap of the relationship between ESTIMATE scores, GSVA, and different cohorts of the two clusters. (**E**–**G**) Differences in the expression of immune infiltrating cells and immune related functions based on ssGSEA and CIBERSORT between the two clusters. (**H**) Expression differences of chemokine related genes between the two clusters. (**I**) Expression differences of immune checkpoint related genes between the two clusters. (**K**–**M**) ESTIMATEcore, StromalScore and TumorPurity for two clusters. (**N**) Volcano plot showing differentially expressed MAPGs in OSCC. (**O**,**P**) GO and KEGG enrichment analysis. $^{*}p < 0.05$, $^{**}p < 0.01$, $^{***}p < 0.001$, $^{****}p < 0.0001$.

Identification of key prognostic MAPG using machine learning approaches

We used nine machine learning algorithms, namely Gradient Boosting (GB), Gradient Boosting with Cross-Validation (GB-CV), Gradient Boosting Machines (GBM), Linear Discriminant Analysis (LDA), Linear Discriminant Analysis with Cross-Validation (LDA-CV), Random Forest (RF), Support Vector Machine (SVM), Support Vector Machine with Cross-Validation (SVM-CV) and LASSO regression to identify the importance of MAPGs (Fig. 4A–J, Table.S2). Based on the nine machine learning algorithms described above, overlapping genes (INHBA, TNFRSF19, and PRKAA2) were selected as potent prognostic factors and visualized using flower plots (Fig. 4K). Their importance was further examined with various algorithms (Fig. 4L–R). Multiple database analyses revealed that TNFRSF19 and PRKAA2 were underexpressed in HNSCC. Survival analysis indicated that patients with low expression of TNFRSF19 and PRKAA2 had a more favorable prognosis. We further validated the expression of INHBA, TNFRSF19, and PRKAA2 using quantitative PCR (qPCR). The results showed that INHBA exhibited the most pronounced differential expression among the three genes. (Fig. S3, Fig. 5C) Consequently, TNFRSF19 and PRKAA2 were excluded, highlighting the more crucial role of INHBA in OSCC. Ultimately, we screened out the pivotal prognostic gene INHBA, which is associated with mitochondrial pan-cell death.

Correlation of INHBA expression with prognosis and biological functions

Through analyses of the TCGA, GSE42743, and GSE75538 databases, along with in vitro qPCR verification, we found that both INHBA protein and mRNA expression levels were significantly elevated in OSCC and HNSCC. Moreover, these levels increased significantly with the progression of OSCC and HNSCC malignancy (Fig. 5A–D). Subsequently, OSCC and HNSCC samples were respectively stratified into high- and low- INHBA-expression subtypes. Survival analysis revealed a negative correlation between INHBA expression and patient survival, with the high-INHBA-expression subgroup exhibiting a poorer prognosis (Fig. 5E–H). GSEA analysis showed that epithelial-mesenchymal transition, angiogenesis, TGF-β signaling, and TNFα signaling via NF-κB pathways were enriched in samples with high INHBA expression (Fig. 5I). Additionally, GO enrichment and KEGG pathway analyses indicated that INHBA was closely associated with molecular metabolism, protein binding, and mitochondrial redox reactions in OSCC (Fig. 5J,K). Therefore, our findings suggested that increased INHBA expression may promote the invasion of OSCC and HNSCC, thus contributing to poorer patient prognosis. The underlying molecular mechanisms, however, warrant further experimental investigation.

INHBA projection and cell communication analysis in OSCC

Analysis of INHBA expression in the scRNA-seq dataset revealed that INHBA was predominantly enriched in fibroblast clusters (Fig. 6.A-C). Additionally, a positive correlation was observed between INHBA and COL1A1 expression (Fig. 6.D), indicating that high INHBA expression may drive OSCC progression and influence prognosis by mediating tumor fibrosis.

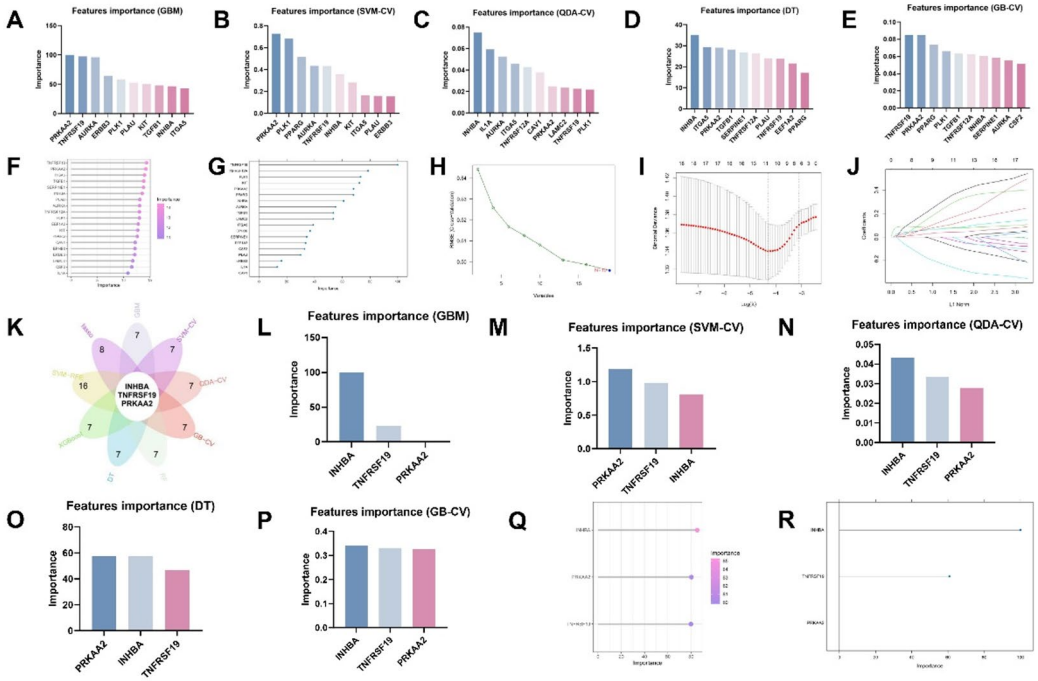

Fig. 4. Screening the most critical MAPG in OSCC using multiple machine learning. (**A**–**J**) Importance of MAPGs evaluated by multiple machine learning algorithms. (**K**) Flower plot showing overlapping genes (INHBA, TNFRSF19 and PRKAA2) based on nine machine learning algorithms. (**L**–**R**) Assessment of the significance of INHBA, TNFRSF19, and PRKAA2 using various machine learning algorithms.

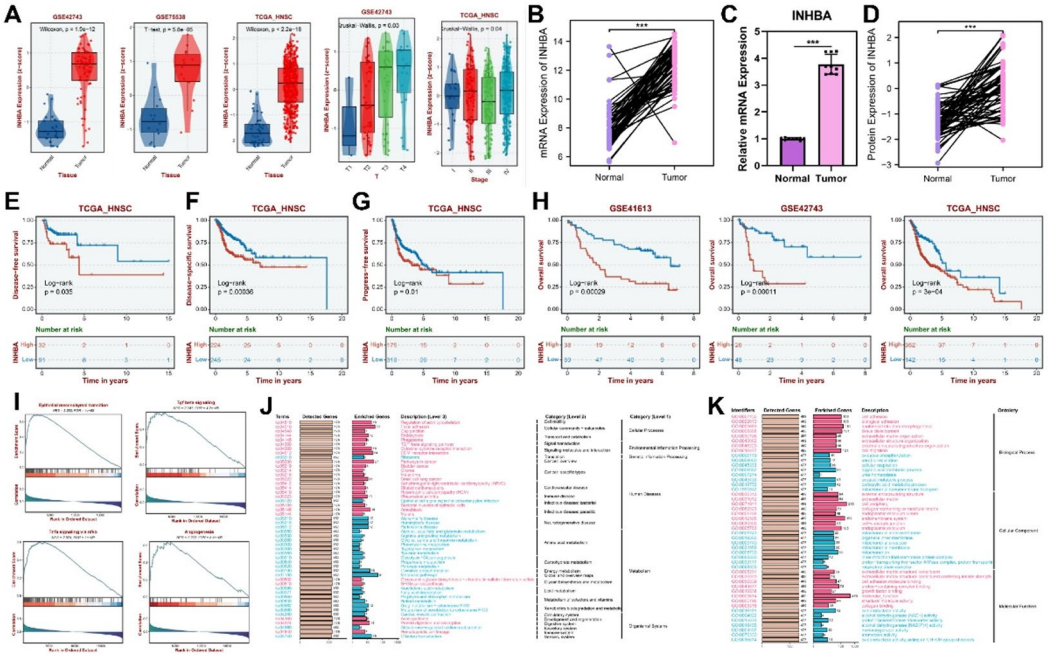

Fig. 5. Expression, prognostic and functional analysis of INHBA. (**A**,**B**,**D**) The expression levels of INHBA in validation set GSE42743, GSE75538 and TCGA_HNSC. (**C**) The expression level of INHBA detected by RT-qPCR in clinical sample. (**E**) Kaplan-Meier curve to show the disease-free survival of HNSCC patients in low INHBA expression and high INHBA expression subgroups. (**F**) Kaplan–Meier Curves for disease-specific survival of INHBA high-expression and INHBA low-expression subgroups. (**G**) Kaplan-Meier curve to show the progress-free survival of HNSCC patients in low INHBA expression and high INHBA expression subgroup. (**H**) Kaplan-Meier curve to show the overall survival of HNSCC patients in low INHBA expression and high INHBA expression subgroups. (**I**) GSEA analyzed gene characteristics between INHBA low expression subgroup and INHBA high expression subgroup, located on the right and left side, respectively. (**J**,**K**) The enrichment of INHBA was analyzed by GO and KEGG. GO, Gene Ontology; KEGG, Kyoto Encyclopedia of Genes and Genomes. $^{*}p<0.05$, $^{**}p<0.01$, $^{***}p<0.001$, $^{****}p<0.0001$.

CellChat was used to map complex intercellular communication networks. In OSCC samples, enhanced interactions were detected between fibroblasts and epithelial cells, as well as between fibroblasts and immune cells (Fig. 6E,I). Ligand-receptor interaction networks among different cell types were analyzed, showing that the PTN-NCL interaction was significantly weakened in OSCC compared to the normal group, whereas the MIF-(CD74 + CXCR4) and MIF-(CD74 + CD44) interactions were notably enhanced (Fig. 6F–H,J–L). Further analysis showed that the communication between fibroblasts and immune cells in MIF-(CD74 + CD44) in tumor group was enhanced. Using spatial transcriptome data, tissue section projections demonstrated the extensive distribution of cancer-associated fibroblasts (CAFs). Overlapping areas of INHBA and CAFs were observed, consistent with single-cell analysis results (Fig. 6M–P). These findings suggested that the intercellular communication patterns in OSCC tissues differ from those in normal cells, and INHBA overexpression may contribute to OSCC development by enhancing communication between tumor fibroblasts and immune cells.

Downstream exploration of fibroblast subsets

Cancer-associated fibroblasts (CAFs) are recognized as pivotal players in the pathogenesis and progression of OSCC. In this study, drawing on previous research[41], we isolated fibroblasts from scRNA-seq data and further classified them into five subgroups: ap-Fibroblast, In-fibroblast, inCAF, myCAF and NF. (Fig. 7A,B, S3). We found that INHBA was expressed in these fibroblast clusters (especially the myCAF clusters) (Fig. 7C,D). Additionally, we observed positive correlations between the expression levels of POSTN, TAGLN, and INHBA (Fig. 7E). CellChat then analyzed intercellular communication within fibroblasts and noted that myCAF/inCAF dominated interactions with other fibroblasts in OSCC, and that this intercellular communication may be mediated mainly by MIF and POSTN regulation (Fig. 7G,H,J). MIF-(CD74CD44) and POSTN-(ITGAV+ITGB5) strongly correlated (Fig. 7K,L). Based on these results, we suggested that the overexpression of INHBA in tumor fibroblasts may regulate the functional relationship between myCAF and inCAF in OSCC, thereby promoting tumor development.

Clinical transformation of INHBA in OSCC

Based on INHBA expression levels, we observed that patients with low INHBA expression exhibited longer overall survival following anti-CTLA4 and anti-PD-L1 treatments. Conversely, those with high INHBA expression showed extended progression-free survival after CAR-T therapy (Fig. 8A–C). These findings

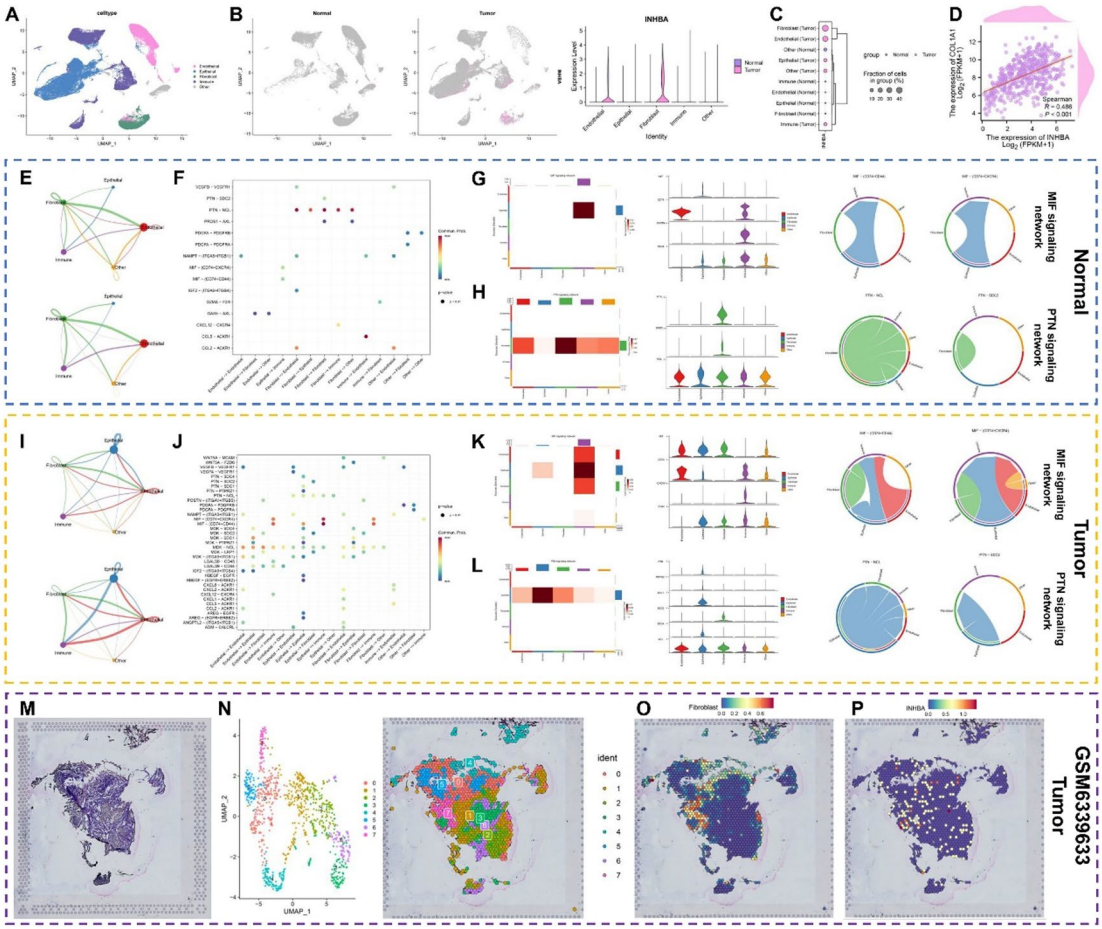

Fig. 6. Analysis of INHBA projection and cell communication in OSCC. (**A**–**C**) The relationship between INHBA expression and different cell clusters in normal and tumor tissues. (**D**) Correlation analysis of COL1A1 and INHBA. (**E**,**I**) Strength and number of ligand-receptor interactions between pairs of cell populations in the normal (**E**) and HNSCC (**I**) groups based on CellChat analysis. (**F**,**J**) Bubble plot of several tumor-specific pathways among different cell clusters in normal (F) and tumor (J) tissues. (G-H) MIF and PTN signaling network shown via heatmap, violin plot, and circle plot in normal tissues. (**K**,**L**) MIF and PTN signaling network shown via heatmap, violin plot and circle plot in tumor tissues. (M-P) The spatial arrangement of INHBA expression and cell clusters via spatial transcriptomics analysis. $^{*}p < 0.05$, $^{**}p < 0.01$, $^{***}p < 0.001$, $^{****}p < 0.0001$.

suggested that CAR-T therapy may be more efficacious in OSCC patients with elevated INHBA expression. After immunotherapy in the GSE195832 database, results showed increased INHBA expression levels, as did Cetuximab for HNSCC (Fig. 8D,E). This suggested that the resistance of Cetuximab may be related to INHBA, and we need to further find suitable drugs for OSCC patients.

Therefore, we analyzed the GDSC and PRISM databases and predicted IC50 drug data. Drug sensitivity analysis revealed that selumetinib and naltrexone were highly sensitive inhibitors of INHBA (Fig. 8F–G,I,J). Subsequently, we conducted a molecular binding study to confirm the binding efficacy of INHBA with these two drugs. The docking results showed that the receptor-ligand binding energy of the core components of selumetinib and naltrexone was ≤ -7.0 kcal/mol, confirming the reliability of our prediction (Fig. 8H,K).

Comprehensive analysis of INHBA in pan-cancer

Pan-cellular death is intricately linked to the initiation and progression of various cancer types. Thus, we sought to determine whether INHBA, the key mitochondria-associated pan-cell death gene (MAPG) identified in this study, could serve as a predictor of poor prognosis across different malignancies. To this end, we analyzed the relative expression of INHBA in 33 cancer types and normal tissue samples from TCGA (Fig. 9A–C). Findings revealed that, compared to normal tissues, INHBA was significantly upregulated in 17 cancer types (BLCA, BRCA, CESC, CHOL, COAD, DLBC, ESCA, GBM, HNSC, KIRC, LAML, LGG, PAAD, PRAD, READ, STAD, and THCA). Conversely, INHBA was downregulated in seven cancer types (ACC, KICH, KIRP, LIHC, SKCM, UCEC, and UCS). We further explored the prognostic value of INHBA across diverse cancer types. Univariate Cox regression analysis of pan-cancer data showed that INHBA upregulation was associated with poor overall survival (OS) in 10 cancer types (ACC, BLCA, CESC, HNSC, KIRP, LAML, LUSC, MESO, PAAD, and STAD)

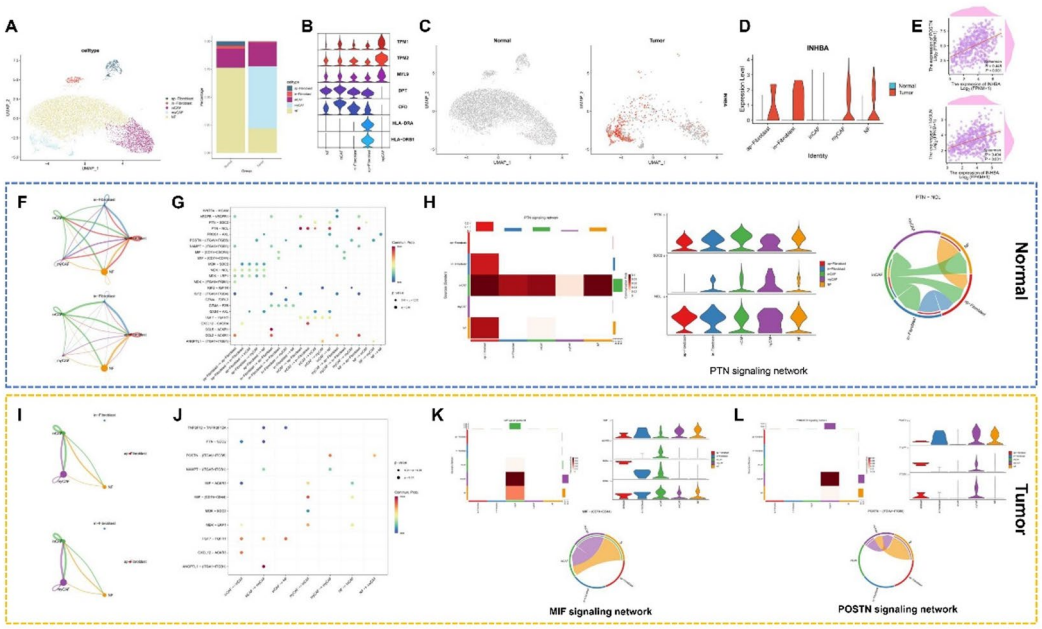

Fig. 7. Downstream exploration of fibroblast subsets. (**A**) UMAP plots for fibroblast subsets in normal and tumor tissues, and bar graph of relative cell proportions. (**B**) Marker genes expressed in 4 major cell compartments. (**C**,**D**) The relationship of INHBA expression and different cell clusters in normal and tumor tissues. (**E**) Correlation analysis of POSTN and TAGLN with INHBA. (**F**,**I**) Strength and number of ligand-receptor interactions between pairs of cell populations in the normal (F) and OSCC (I) groups based on CellChat analysis. (**G**,**J**) Bubble plot of several tumor-specific pathways among different cell clusters in normal (**G**) and tumor (**J**) tissues. (**H**) PTN signaling network shown via heatmap, violin plot, and circle plot in normal tissues. (K-L) MIF and POSTN signaling network shown via heatmap, violin plot and circle plot in tumor tissues. $^{*}p < 0.05$, $^{**}p < 0.01$, $^{***}p < 0.001$, $^{****}p < 0.0001$.

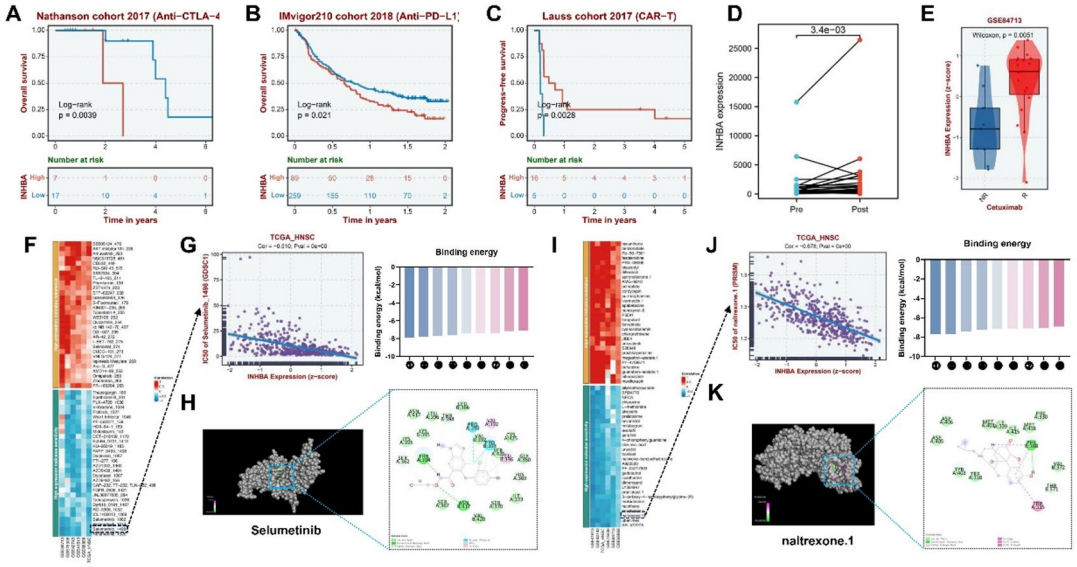

Fig. 8. Clinical transformation of INHBA in OSCC. (**A**–**D**) Kaplan-Meier curves showing the relationship between INHBA expression and survival in the OSCC immunotherapy cohorts. (**E**) Relationship between INHBA expression and cetuximab treatment. (**F**,**I**) Plot of correlation analysis between INHBA expression and several drug sensitivities (IC50) in two databases: GDSC and PRISM. A positive correlation is represented in blue, indicating that increased gene expression corresponds to greater drug sensitivity, whereas red indicates the contrary. (**G**) Relationship between INHBA expression and selumetinib sensitivity. (**J**) Relationship between INHBA expression and naltrexone sensitivity. (H, K) Molecular docking structure diagram of INHBA and two drugs with the highest binding affinities. $^{*}p < 0.05$, $^{**}p < 0.01$, $^{***}p < 0.001$, $^{****}p < 0.0001$.

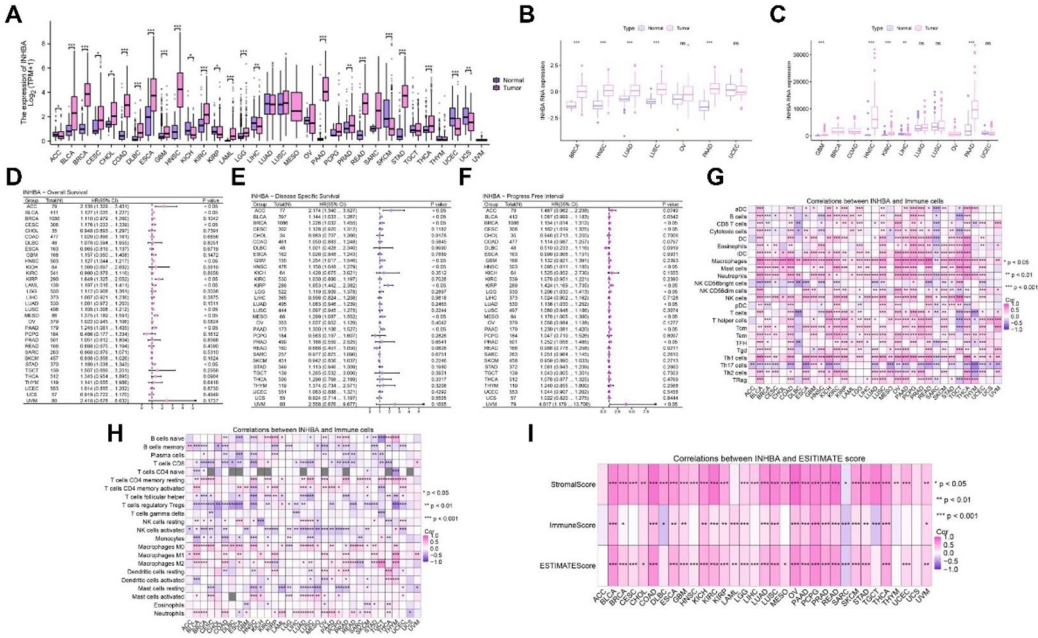

Fig. 9. Comprehensive analysis of INHBA in pan-cancers. (**A**–**C**) INHBA expression in 33 tumor types. (**D**–**F**) Prognosis of INHBA in 33 tumors. (**G**,**H**) Analysis of immune cell infiltration in 33 tumors based on INHBA. (**I**) ImmuneScore, StromalScore, and ESTIMATEScore scores in 33 tumors based on INHBA. $^{*}p < 0.05$, $^{**}p < 0.01$, $^{***}p < 0.001$, $^{****}p < 0.0001$.

(Fig. 9D). In eight cancer types (ACC, BLCA, BRCA, GBM, HNSC, KIRP, MESO, and PAAD), INHBA upregulation was linked to poor disease-free survival (DSS) (Fig. 9E). Additionally, in 10 cancer types (BRCA, CESC, HNSC, KIRP, LGG, LUAD, MESO, PAAD, PRAD, and UVM), INHBA upregulation correlated with a poor progression-free interval (Fig. 9F).

We also investigated the association between INHBA gene expression and tumor microenvironment. The results showed that INHBA expression was closely associated with the infiltration levels of macrophages, neutrophils, and Th1 cells in multiple tumors (Fig. 9G,H). Using the ESTIMATE algorithm to quantify the immune and stromal scores, we found that INHBA gene expression was significantly correlated with the stromal score in most cancer types (Fig. 9I).

Discussion

Oral squamous cell carcinoma (OSCC), a common subtype of head and neck cancer, is characterized by high recurrence rates and poor survival[42,43]. The pathogenesis and progression of OSCC involve intricate molecular alterations. Despite significant advancements in treatment and diagnostic strategies, the overall survival rate for OSCC patients remains suboptimal[44]. Consequently, there is an urgent imperative to identify robust and clinically relevant biomarkers or regulatory genes to facilitate the development of personalized treatment plans for OSCC patients and achieve durable therapeutic outcomes. Mitochondrial-related genes govern extensive signal transduction networks and regulate diverse cell death mechanisms[45,46]. The dysregulation of mitochondria-associated pan-cell death has been implicated in the etiology of various diseases[47,48]. However, the roles and mechanisms of mitochondria-associated pan-cell death genes (MAPGs) in OSCC remain poorly understood. Moreover, the specific MAPGs that may exert a pivotal influence on OSCC progression have yet to be elucidated.

INHBA, a mitochondria-associated pan-cell death gene and member of the transforming growth factor-β (TGF-β) superfamily, exhibits multifunctional roles in immune responses, fibroblast activation, and regulation of cell migration and proliferation[49,50]. Accumulating evidence supports its involvement in multiple cancer types[51,52]. For instance, Li et al. reported that INHBA promotes tumor progression by suppressing IFN-γ signaling and conferring resistance to PD-L1 blockade[53]. Similarly, Liu et al. demonstrated that INHBA knockout in breast cancer cells suppressed proliferation, reduced invasiveness, and enhanced sensitivity to lapatinib[54]. In this study, we applied multiple machine learning algorithms to enhance the reliability of gene selection and identified INHBA as a pivotal mitochondria-associated pan-cell death gene (MAPG) in OSCC. We found that INHBA was overexpressed in OSCC, and the high expression of INHBA was closely related to the poor prognosis of OSCC. This prognostic role of INHBA was also observed in the broader cohort of HNSCC patients. Through GSEA, GO, and KEGG analyses, we further revealed that INHBA may facilitate OSCC progression by promoting angiogenesis and epithelial-mesenchymal transition, potentially via modulation of mitochondrial oxidative stress. Pan-cancer analysis corroborated that INHBA overexpression correlates with poor overall survival across multiple malignancies. Additionally, INHBA expression showed significant positive correlations with StromalScore, ImmuneScore, and ESTIMATEscore, underscoring its close relationship with

the tumor immune microenvironment. Furthermore, elevated INHBA expression was correlated with increased infiltration of pro-tumor immune cells, such as macrophages and neutrophils, suggesting a potential role in shaping an immunosuppressive microenvironment. However, further clinical validation is required to confirm these findings. In summary, INHBA played a dual role as a potential immunotherapy target and a predictive biomarker in OSCC, and may hold clinical value for targeted therapy in cancers such as HNSCC. Mechanistically, INHBA appeared to drive OSCC progression, at least in part, by remodeling the immune microenvironment.

To further investigate the cellular heterogeneity of INHBA in OSCC, we compared single-cell transcriptomic profiles between tumor and normal samples, which revealed predominant enrichment of INHBA in fibroblast clusters and a positive correlation with COL1A1 expression. As a key extracellular matrix (ECM) component, COL1A1 participates in multiple biological processes[55]. Previous studies have demonstrated that fibroblast-derived COL1A1 promotes ovarian cancer metastasis via ITGB1/AKT signaling activation[56], and that COL1A1-CD44 interaction mediates fibroblast-malignant cell crosstalk in HNSCC, fostering a tumor-promoting microenvironment[57]. These findings support the hypothesis that INHBA-high cancer-associated fibroblasts may facilitate OSCC progression through enhanced COL1A1 secretion. Cell-cell communication analysis further identified strengthened interactions in OSCC, particularly between fibroblasts and epithelial or immune cells, with the MIF-(CD74 + CD44) axis emerging as a notably enhanced pathway. MIF is a representative pro-inflammatory factor that plays a role in regulating immune response[58]. Studies had shown that high expression of MIF could promote tumor progression and metastasis, stimulate angiogenesis, and create an immunosuppressive microenvironment conducive to tumor development[59]. Thus, INHBA may promote the development of OSCC by enhancing the effect of MIF ligands on the CD74-CD44 receptor, facilitating the interaction between fibroblasts and immune cells, and regulating the immune microenvironment of OSCC.

Cancer-associated fibroblasts (CAFs), the most abundant stromal cells in the tumor microenvironment, comprise distinct subpopulations derived from heterogeneous cell types and are implicated in mediating poor tumor prognosis[60]. In this study, drawing on previous literature[41], we classified CAFs into five clusters and observed a significant increase in myCAF clusters in OSCC. Notably, INHBA was predominantly enriched in myCAFs and exhibited positive correlations with POSTN and TAGLN expression. Previous studies had implicated myCAFs in extracellular matrix remodeling and metastasis[61], and suggested their role in shaping a metastatic niche via paracrine signaling in HNSCC[62]. POSTN and TAGLN had been shown to be carcinogenic mRNAs in many types of cancer[63,64]. For instance, Yu et al. demonstrated that CAF-derived POSTN promotes cancer stemness through interaction with PTK7 in HNSCC[65], while Sarubo et al. reported that TAGLN upregulation enhances stem-like properties and tumor progression[66]. Moreover, Wang et al. revealed that $POSTN^+$ CAFs suppress $CD8^+$ T cell infiltration, foster an immunosuppressive microenvironment, and impair response to immunotherapy[67]. Our cell-cell communication analysis further revealed that the myCAF/inCAF subset predominantly mediates interactions with other fibroblast populations in OSCC. Specifically, myCAF/inCAF crosstalk was largely driven by MIF signaling, whereas intracellular communication within myCAFs was regulated by POSTN. These findings collectively suggested that INHBA may exert its pro-tumor effects primarily through myCAFs, remodeling the metastatic niche and promoting OSCC progression. Additionally, these results highlighted the therapeutic potential of targeting myCAF subpopulations in OSCC treatment.

A profound understanding of the key targets and functionally pivotal cell subgroups in OSCC could facilitate more precise treatment strategies and improve patient survival rates. In our study, we initially discovered that anti-PD-L1, anti-CTLA4 immunotherapies, and cetuximab may not confer favorable prognoses for HNSCC patients with high INHBA expression. Conversely, CAR-T therapy appeared to offer greater benefits to this patient subgroup. Given that immunotherapy alone was insufficient to counteract the complex and highly heterogeneous tumor microenvironment of OSCC, adjunctive drug therapy was crucial for optimizing patient outcomes. Subsequently, we analyzed the correlations between INHBA expression and predicted IC50 drug data from the GDSC and PRISM databases. Our findings indicated that selumetinib and naltrexone exhibited the most promising potential efficacy in the OSCC subclass with high INHBA expression. Selumetinib, a highly specific mitogen-activated protein kinase 1/2 inhibitor, had shown promising results in preclinical and clinical trials as a single agent or in combination with conventional chemotherapy and other targeted therapies for a variety of cancers, including childhood low-grade glioma, non-small cell lung cancer, and melanoma[68,69]. Feng et al. showed that Selumetinib is an effective compound for patients with high-risk squamous cell carcinoma[70]. Naltrexone is a nonspecific opioid antagonist that exerts pharmacological effects on the opioid axis by blocking opioid receptors distributed in cytoplasmic and nuclear regions[71]. Liu et al. found that low-dose naltrexone delayed the development of cervical cancer by inhibiting the PI3K/AKT/mTOR pathway[72]. Gorur et al. found that low doses of methylnaltrexone inhibited the growth and development of HNSCC in vivo and in vitro[73]. According to our study results, the core components of selumetinib and naltrexone exhibited strong binding affinity to key target proteins, validating the reliability of our predictions. We propose that selumetinib and naltrexone may enhance the anti-tumor efficacy and improve the survival of OSCC patients by downregulating INHBA expression. Moreover, given the significant role of INHBA across multiple cancer types, therapeutic targeting of INHBA may represent a promising strategy with potential clinical utility in multiple malignancies, particularly in HNSCC.

This study systematically characterizes the prognostic and mechanistic significance of mitochondrial-associated pan-cell death-related genes (MAPGs) in OSCC through integrated multi-omics profiling and machine learning. Unlike previous studies, our work uniquely identifies INHBA as an important regulator in OSCC and delineates its cell-type-specific expression, primarily within myofibroblastic cancer-associated fibroblasts (myCAFs). We further demonstrate that INHBA may modulate CAF-immune cell crosstalk via the MIF signaling pathway, thereby reshaping the immune microenvironment and influencing tumor progression and patient prognosis. Notably, we pinpoint two FDA-approved agents, selumetinib and naltrexone, as potential INHBA-targeting inhibitors, generating hypotheses for future experimental testing and potential repurposing.

Overall, our research findings link mechanism understanding with clinical practicality, providing a new approach for advancing the management of OSCC.

Conclusions

In this study, we integrated multi-center, multi-omics, and in-depth bioinformatic analyses to delineate the prognostic relevance and functional significance of mitochondria-associated pan-cell death genes (MAPGs) in OSCC, while systematically characterizing the tumor microenvironment (TME) landscape. By leveraging multiple machine learning algorithms, we identified INHBA as a central MAPG and elucidated its critical role in OSCC pathogenesis. We further demonstrated that INHBA was primarily active within tumor-associated fibroblasts, particularly myofibroblastic CAFs (myCAFs), where it contributed to immune microenvironment remodeling and promoted tumor progression. Additionally, our results suggested that OSCC patients with high INHBA expression may respond more favorably to CAR-T immunotherapy, and that selumetinib and naltrexone represent promising targeted therapeutic options for this patient subgroup. Meanwhile, INHBA was implicated in multiple malignancies, including HNSCC, suggesting that targeting INHBA may represent a broadly applicable therapeutic strategy with potential clinical utility across multiple malignancies.

Data availability

Publicly available datasets were analyzed in this study. The clinical information and expression data of 502 HNSCC tissues, 44 adjacent normal tissues and corresponding clinical data were downloaded from the Cancer Genome Atlas (TCGA) (http://cancergenome.nih.gov/) database. GSO datasets (GSE42743, GSE41613 and GSE 75538) were downloaded from the GEO (https://www.ncbi.nlm.nih.gov/) database. Single-cell RNA sequencing data were obtained from GEO databases (GSE164241 and GSE172577) and included 8 normal buccal mucosa samples and 6 oral squamous cell carcinoma samples. Spatial transcriptome data were obtained from geo database (GSM6339633). The datasets generated during and/or analyzed during the current study are available from the corresponding author on reasonable request.

Received: 21 October 2025; Accepted: 29 January 2026
Published online: 25 February 2026

References

1. Johnson, D. E. et al. Head and neck squamous cell carcinoma. *Nat. Rev. Dis. Primers*. **6**, 92. https://doi.org/10.1038/s41572-020-00224-3 (2020).
2. Tandon, P., Dadhich, A., Saluja, H., Bawane, S. & Sachdeva, S. The prevalence of squamous cell carcinoma in different sites of oral cavity at our rural health care centre in Loni, Maharashtra - a retrospective 10-year study. *Contemp. Oncol. (Pozn)*. **21**, 178–183. https://doi.org/10.5114/wo.2017.68628 (2017).
3. Tan, Y. et al. Oral squamous cell carcinomas: state of the field and emerging directions. *Int. J. Oral Sci.* **15**, 44. https://doi.org/10.1038/s41368-023-00249-w (2023).
4. Linsen, S. S., Gellrich, N. C. & Kruskemper, G. Age- and localization-dependent functional and psychosocial impairments and health related quality of life six months after OSCC therapy. *Oral Oncol.* **81**, 61–68. https://doi.org/10.1016/j.oraloncology.2018.04.011 (2018).
5. Romano, A. et al. Noninvasive imaging methods to improve the diagnosis of oral carcinoma and its precursors: state of the Art and proposal of a Three-Step diagnostic process. *Cancers (Basel)*. 13. https://doi.org/10.3390/cancers13122864 (2021).
6. Shen, Y. et al. CDK5RAP2 is a Wnt target gene and promotes stemness and progression of oral squamous cell carcinoma. *Cell. Death Dis.* **14** https://doi.org/10.1038/s41419-023-05652-z (2023).
7. Li, C., Dong, X. & Li, B. Tumor microenvironment in oral squamous cell carcinoma. *Front. Immunol.* **15**, 1485174. https://doi.org/10.3389/fimmu.2024.1485174 (2024).
8. Ran, J. et al. Rhythm Mild-Temperature photothermal therapy enhancing Immunogenic cell death response in oral squamous cell carcinoma. *Adv. Healthc. Mater.* **12**, e2202360. https://doi.org/10.1002/adhm.202202360 (2023).
9. Sun, Y. et al. GSH/pH-responsive copper-based cascade nanocomplexes inducing Immunogenic cell death through cuproptosis/ferroptosis/necroptosis in oral squamous cell carcinoma. *Mater. Today Bio*. **30**, 101434. https://doi.org/10.1016/j.mtbio.2024.101434 (2025).
10. Gupta, S., Singh, A., Deorah, S. & Tomar, A. Immunotherapy in OSCC: current trend and challenges. *Crit. Rev. Oncol. Hematol.* **209**, 104672. https://doi.org/10.1016/j.critrevonc.2025.104672 (2025).
11. Jiang, Y., Cheng, J., Wu, J., Liu, O. & Bin, X. Innate immune cells in oral squamous cell carcinoma: characteristics and therapeutic potential. *Biochim. Biophys. Acta Rev. Cancer*. **1880**, 189444. https://doi.org/10.1016/j.bbcan.2025.189444 (2025).
12. Gu, W. et al. Multi-omics analysis of ferroptosis regulation patterns and characterization of tumor microenvironment in patients with oral squamous cell carcinoma. *Int. J. Biol. Sci.* **17**, 3476–3492. https://doi.org/10.7150/ijbs.61441 (2021).
13. Ethiraj, P. et al. RANKL triggers resistance to TRAIL-induced cell death in oral squamous cell carcinoma. *J. Cell. Physiol.* **235**, 1663–1673. https://doi.org/10.1002/jcp.29086 (2020).
14. Meng, Y., Chen, Q., Zhou, Z. & Li, M. Regulated cell death in cancer: Mechanisms, crosstalk, and opportunities for therapy. *Cancer Lett.* **635**, 218077. https://doi.org/10.1016/j.canlet.2025.218077 (2025).
15. Zhuang, D. et al. Phenformin activates ER stress to promote autophagic cell death via NIBAN1 and DDIT4 in oral squamous cell carcinoma independent of AMPK. *Int. J. Oral Sci.* **16**, 35. https://doi.org/10.1038/s41368-024-00297-w (2024).
16. Xia, L. et al. Receptor accessory protein 6, a novel ferroptosis suppressor, drives oral squamous cell carcinoma by maintaining Endoplasmic reticulum hemostasis. *Int. J. Biol. Macromol.* **283**, 137565. https://doi.org/10.1016/j.ijbiomac.2024.137565 (2024).
17. Glover, H. L., Schreiner, A., Dewson, G. & Tait, S. W. G. Mitochondria and cell death. *Nat. Cell. Biol.* **26**, 1434–1446. https://doi.org/10.1038/s41556-024-01429-4 (2024).
18. Marquez-Jurado, S. et al. Mitochondrial levels determine variability in cell death by modulating apoptotic gene expression. *Nat. Commun.* **9**, 389. https://doi.org/10.1038/s41467-017-02787-4 (2018).
19. Bliksoen, M. et al. Extracellular MtDNA activates NF-kappaB via toll-like receptor 9 and induces cell death in cardiomyocytes. *Basic. Res. Cardiol.* **111** https://doi.org/10.1007/s00395-016-0553-6 (2016).
20. Diao, P. et al. Integrative multiomics analyses identify molecular subtypes of head and neck squamous cell carcinoma with distinct therapeutic vulnerabilities. *Cancer Res.* **84**, 3101–3117. https://doi.org/10.1158/0008-5472.CAN-23-3594 (2024).
21. He, D. et al. Multi-omics and machine learning-driven CD8(+) T cell heterogeneity score for head and neck squamous cell carcinoma. *Mol. Ther. Nucleic Acids*. **36**, 102413. https://doi.org/10.1016/j.omtn.2024.102413 (2025).

22. Shi, L. et al. Multi-Omics reveal the metabolic changes in cumulus cells during aging. *Cell. Prolif.* **e70014** https://doi.org/10.1111/cpr.70014 (2025).
23. Yang, Z. et al. A comprehensive study based on exosome-related immunosuppression genes and tumor microenvironment in hepatocellular carcinoma. *BMC Cancer*. **22**, 1344. https://doi.org/10.1186/s12885-022-10463-0 (2022).
24. Reed, E. R. & Monti, S. Multi-resolution characterization of molecular taxonomies in bulk and single-cell transcriptomics data. *Nucleic Acids Res.* **49**, e98. https://doi.org/10.1093/nar/gkab552 (2021).
25. Zha, X. Bioinformatics analysis techniques identify the ferroptosis-related genemycas a potential therapeutic target for spinal cord injury: an observational study based on the GEO database. *Adv. Technol. Neurosci.* **2**, 59–71 (2025).
26. Hao, J. et al. Single-cell multi-omics Deciphers hepatocyte dedifferentiation and illuminates maintenance strategies. *Cell. Prolif.* **58**, e13772. https://doi.org/10.1111/cpr.13772 (2025).
27. Tao, W. et al. Discovering DISCO: application value of a large-scale repository for diverse single-cell omics Dat. *Adv. Technol. Neurosci.* **2**, 116–121. https://doi.org/10.4103/atn.Atn-d-24-00035 (2025).
28. Huang, C., Zhu, F., Zhang, H., Wang, N. & Huang, Q. Identification of S1PR4 as an immune modulator for favorable prognosis in HNSCC through machine learning. *iScience* **26**, 107693. https://doi.org/10.1016/j.isci.2023.107693 (2023).
29. Zhao, A. R., Yuan, R., Kouznetsova, V. L. & Tsigelny, I. F. Application of machine learning technology and MiRNA biomarkers: A novel approach for epilepsy diagnosis. *Adv. Technol. Neurosci.* **2**, 145–151. https://doi.org/10.4103/atn.Atn-d-25-00017 (2025).
30. Si, J. et al. tRF-3a-Pro: A transfer RNA-Derived small RNA as a novel biomarker for diagnosis of hepatitis B Virus-Related hepatocellular carcinoma. *Cell. Prolif.* https://doi.org/10.1111/cpr.70006 (2025).
31. Henn, A. D. et al. Smart biomanufacturing for health equity in regenerative medicine therapies. *Regenerative Med. Rep.* **2**, 31–35 (2025).
32. Francis, J., George, J., Peng, E. & Corno, A. F. The application of artificial intelligence in tissue repair and regenerative medicine related to pediatric and congenital heart surgery: a narrative review. *Regenerative Med. Rep.* **1**, 131–136. https://doi.org/10.4103/regenmed.Regenmed-d-24-00013 (2024).
33. Sun, M. et al. Cuproptosis-related LncRNA JPX regulates malignant cell behavior and epithelial-immune interaction in head and neck squamous cell carcinoma via miR-193b-3p/PLAU axis. *Int. J. Oral Sci.* **16**, 63. https://doi.org/10.1038/s41368-024-00314-y (2024).
34. Rath, S. et al. MitoCarta3.0: an updated mitochondrial proteome now with sub-organelle localization and pathway annotations. *Nucleic Acids Res.* **49**, D1541–D1547. https://doi.org/10.1093/nar/gkaa1011 (2021).
35. Qin, H. et al. Integrated machine learning survival framework develops a prognostic model based on inter-crosstalk definition of mitochondrial function and cell death patterns in a large multicenter cohort for lower-grade glioma. *J. Transl Med.* **21**, 588. https://doi.org/10.1186/s12967-023-04468-x (2023).
36. Subramanian, A. et al. Gene set enrichment analysis: a knowledge-based approach for interpreting genome-wide expression profiles. *Proc. Natl. Acad. Sci. U S A.* **102**, 15545–15550. https://doi.org/10.1073/pnas.0506580102 (2005).
37. Williams, D. W. et al. Human oral mucosa cell atlas reveals a stromal-neutrophil axis regulating tissue immunity. *Cell* **184**, 4090–4104 e4015. https://doi.org/10.1016/j.cell.2021.05.013 (2021).
38. Li, H. et al. Mature tertiary lymphoid structures evoke intra-tumoral T and B cell responses via progenitor exhausted CD4(+) T cells in head and neck cancer. *Nat. Commun.* **16**, 4228. https://doi.org/10.1038/s41467-025-59341-w (2025).
39. Jin, S. et al. Inference and analysis of cell-cell communication using cellchat. *Nat. Commun.* **12**, 1088. https://doi.org/10.1038/s41467-021-21246-9 (2021).
40. Lou, Y. et al. Ultraviolet Light-Based micropattern printing on titanium surfaces to promote early osseointegration. *Adv. Healthc. Mater.* **12**, e2203300. https://doi.org/10.1002/adhm.202203300 (2023).
41. Gao, Y. et al. Cross-tissue human fibroblast atlas reveals myofibroblast subtypes with distinct roles in immune modulation. *Cancer Cell.* **42** (1764–1783 e1710). https://doi.org/10.1016/j.ccell.2024.08.020 (2024).
42. Knochelmann, H. M. et al. Neoadjuvant presurgical PD-1 Inhibition in oral cavity squamous cell carcinoma. *Cell. Rep. Med.* **2**, 100426. https://doi.org/10.1016/j.xcrm.2021.100426 (2021).
43. Zhang, X. et al. MF-094 nanodelivery inhibits oral squamous cell carcinoma by targeting USP30. *Cell. Mol. Biol. Lett.* **27**, 107. https://doi.org/10.1186/s11658-022-00407-8 (2022).
44. Borsetto, D. et al. Prognostic significance of CD4 + and CD8 + Tumor-Infiltrating lymphocytes in head and neck squamous cell carcinoma: A Meta-Analysis. *Cancers (Basel)*. **13** https://doi.org/10.3390/cancers13040781 (2021).
45. Poltorak, A. Cell death: all roads lead to mitochondria. *Curr. Biol.* **32**, R891–R894. https://doi.org/10.1016/j.cub.2022.07.025 (2022).
46. Ding, Z. et al. Mitochondrial regulation of ferroptosis in cancer cells. *Int. J. Biol. Sci.* **21**, 2179–2200. https://doi.org/10.7150/ijbs.105446 (2025).
47. Tian, C., Liu, Y., Li, Z., Zhu, P. & Zhao, M. Mitochondria related cell death modalities and disease. *Front. Cell. Dev. Biol.* **10**, 832356. https://doi.org/10.3389/fcell.2022.832356 (2022).
48. Ma, F. et al. Exploring the therapeutic potential of MIR-140-3p in osteoarthritis: targeting CILP and ferroptosis for novel treatment strategies. *Cell. Prolif.* **e70018** https://doi.org/10.1111/cpr.70018 (2025).
49. Hu, Y. et al. INHBA(+) cancer-associated fibroblasts generate an immunosuppressive tumor microenvironment in ovarian cancer. *NPJ Precis Oncol.* **8** https://doi.org/10.1038/s41698-024-00523-y (2024).
50. Zhang, S., Jin, K., Li, T., Zhou, M. & Yang, W. Comprehensive analysis of INHBA: A biomarker for anti-TGFbeta treatment in head and neck cancer. *Exp. Biol. Med. (Maywood)*. **247**, 1317–1329. https://doi.org/10.1177/15353702221085203 (2022).
51. Li, X. et al. INHBA is a prognostic predictor for patients with colon adenocarcinoma. *BMC Cancer*. **20**, 305. https://doi.org/10.1186/s12885-020-06743-2 (2020).
52. Liu, F. et al. Identification of INHBA as a potential biomarker for gastric cancer through a comprehensive analysis. *Sci. Rep.* **13**, 12494. https://doi.org/10.1038/s41598-023-39784-1 (2023).
53. Li, F. L. et al. INHBA promotes tumor growth and induces resistance to PD-L1 Blockade by suppressing IFN-gamma signaling. *Acta Pharmacol. Sin.* **46**, 448–461. https://doi.org/10.1038/s41401-024-01381-x (2025).
54. Liu, M. et al. INHBA is a mediator of aggressive tumor behavior in HER2 + basal breast cancer. *Breast Cancer Res.* **24** https://doi.org/10.1186/s13058-022-01512-4 (2022).
55. Devos, H., Zoidakis, J., Roubelakis, M. G., Latosinska, A. & Vlahou, A. Reviewing the regulators of COL1A1. *Int. J. Mol. Sci.* **24** https://doi.org/10.3390/ijms241210004 (2023).
56. Li, M. et al. Microenvironment remodeled by tumor and stromal cells elevates fibroblast-derived COL1A1 and facilitates ovarian cancer metastasis. *Exp. Cell. Res.* **394**, 112153. https://doi.org/10.1016/j.yexcr.2020.112153 (2020).
57. Sosa, J. & Sinha, S. Abstract 5231: follistatin shapes the tumor microenvironment in head and neck squamous cell carcinoma through COL1A1-CD44-mediated tumor-stroma crosstalk. *Cancer Res.* 85 (2025).
58. Li, S. et al. Integrative multi-omics analysis reveals a novel subtype of hepatocellular carcinoma with biological and clinical relevance. *Front. Immunol.* **15**, 1517312. https://doi.org/10.3389/fimmu.2024.1517312 (2024).
59. Zhao, Z., Jia, H., Sun, Z., Li, Y. & Liu, L. A new perspective on macrophage-targeted drug research: the potential of KDELR2 in bladder cancer immunotherapy. *Front. Immunol.* **15**, 1485109. https://doi.org/10.3389/fimmu.2024.1485109 (2024).
60. Lavie, D., Ben-Shmuel, A., Erez, N. & Scherz-Shouval, R. Cancer-associated fibroblasts in the single-cell era. *Nat. Cancer*. **3**, 793–807. https://doi.org/10.1038/s43018-022-00411-z (2022).

61. Du, Y. et al. Dynamic changes in myofibroblasts affect the carcinogenesis and prognosis of bladder cancer associated with tumor microenvironment remodeling. *Front. Cell. Dev. Biol.* **10**, 833578. https://doi.org/10.3389/fcell.2022.833578 (2022).
62. Zeltz, C. et al. α11β1 integrin is induced in a subset of Cancer-Associated fibroblasts in desmoplastic tumor stroma and mediates in vitro cell migration. *Cancers (Basel)*. **11**, 765. https://doi.org/10.3390/cancers11060765 (2019).
63. Yu, Y., Tan, C. M. & Jia, Y. Y. Research status and the prospect of POSTN in various tumors. *Neoplasma* **68**, 673–682. https://doi.org/10.4149/neo_2021_210223N239 (2021).
64. Han, M. Z. et al. TAGLN2 is a candidate prognostic biomarker promoting tumorigenesis in human gliomas. *J. Exp. Clin. Cancer Res.* **36**, 155. https://doi.org/10.1186/s13046-017-0619-9 (2017).
65. Yu, B. et al. Periostin secreted by cancer-associated fibroblasts promotes cancer stemness in head and neck cancer by activating protein tyrosine kinase 7. *Cell. Death Dis.* **9**, 1082. https://doi.org/10.1038/s41419-018-1116-6 (2018).
66. Sarubo, M. et al. Involvement of TGFBI-TAGLN axis in cancer stem cell property of head and neck squamous cell carcinoma. *Sci. Rep.* **14**, 6767. https://doi.org/10.1038/s41598-024-57478-0 (2024).
67. Wang, H. et al. POSTN(+) cancer-associated fibroblasts determine the efficacy of immunotherapy in hepatocellular carcinoma. *J. Immunother Cancer*. **12** https://doi.org/10.1136/jitc-2023-008721 (2024).
68. Campagne, O., Yeo, K. K., Fangusaro, J. & Stewart, C. F. Clinical pharmacokinetics and pharmacodynamics of selumetinib. *Clin. Pharmacokinet.* **60**, 283–303. https://doi.org/10.1007/s40262-020-00967-y (2021).
69. Liu, C. et al. Ultraviolet radiant Energy-Dependent functionalization regulates cellular behavior on titanium dioxide nanodots. *ACS Appl. Mater. Interfaces*. **12**, 31793–31803. https://doi.org/10.1021/acsami.0c07761 (2020).
70. Feng, B. et al. Prognostic gene signature for squamous cell carcinoma with a higher risk for treatment failure and accelerated MEK-ERK pathway activity. *Cancers (Basel)*. 13. https://doi.org/10.3390/cancers13205182 (2021).
71. Qu, N., Meng, Y., Handley, M. K., Wang, C. & Shan, F. Preclinical and clinical studies into the bioactivity of low-dose Naltrexone (LDN) for oncotherapy. *Int. Immunopharmacol.* **96**, 107714. https://doi.org/10.1016/j.intimp.2021.107714 (2021).
72. Liu, N. et al. Low-dose Naltrexone plays antineoplastic role in cervical cancer progression through suppressing PI3K/AKT/mTOR pathway. *Transl Oncol.* **14**, 101028. https://doi.org/10.1016/j.tranon.2021.101028 (2021).
73. Gorur, A. et al. Low doses of Methylnaltrexone inhibits head and neck squamous cell carcinoma growth in vitro and in vivo by acting on the mu-opioid receptor. *J. Cell. Physiol.* **236**, 7698–7710. https://doi.org/10.1002/jcp.30421 (2021).

Author contributions

X.Z, and J.L contributed to the conception and design. X.Z, and M.S collected and analyzed the data. J.L., T.Q., D.H, and T.Z drew the figures and tables. X.Z, J.L., and M.S wrote the draft. X.Z, and J.L contributed to manuscript writing and revision. All authors read and approved the final manuscript.

Funding

This work was financially supported by the following programs: National Natural Science Foundation of China (82501180), Natural Science Foundation of Zhejiang Province (LQN25H140004), Zhejiang Province Traditional Chinese Medicine Science and Technology Plan Project (2026ZL0078), Zhejiang Provincial Medical and Health Science and Technology Plan (2025HY0609, 2025KY942), China Postdoctoral Science Foundation (2024T170782, 2023M743009), Zhejiang University of Stomatology Postdoctoral Scientific Research Foundation (2023PDF013).

Declarations

Competing interests

The authors declare no competing interests.

Ethical approval

This study was performed in line with the principles of the Declaration of Helsinki. Patients who volunteered to take part in the study gave their written informed permission. This study was approved by the Human Research Ethics Committee of the Second Affiliated Hospital of Zhejiang University School of Medicine (Ethics No. 20250631).

Additional information

Supplementary Information The online version contains supplementary material available at https://doi.org/10.1038/s41598-026-38131-4.

Correspondence and requests for materials should be addressed to M.S. or J.L.